

Determination of *B*-cation chemical short-range order in perovskites from the total pair-distribution function

Victor Krayzman^{a,b} and Igor Levin^{a*}

^aCeramics Division, National Institute of Standards and Technology, Gaithersburg, MD 20899, USA, and ^bDepartment of Materials and Nuclear Engineering, University of Maryland, College Park, MD 20742, USA. Correspondence e-mail: igor.levin@nist.gov

Short-range *B*-cation order affects the functional properties of many complex perovskites. However, current ability to measure the characteristics of such chemical short-range order (SRO) in perovskite-structured ceramics is limited. In the present study, two distinct methods are compared for the determination of the *B*-cation SRO parameters from the total scattering pair-distribution function (PDF). Both methods rely on reverse Monte Carlo refinements of the structural models but differ in the procedures used to extract the SRO characteristics. The accuracy of these methods was tested using synthetic PDF data generated for models of prototype $\text{Ca}(\text{Zr,Ti})\text{O}_3$ solid solutions. One of the approaches developed in the present study, which proved to yield the most accurate results, was used to analyze the SRO of Ti and Zr in powder samples of $\text{Ca}(\text{Zr,Ti})\text{O}_3$.

© 2008 International Union of Crystallography
Printed in Singapore – all rights reserved

1. Introduction

Complex perovskite-like compounds $A(B',B'')\text{O}_3$ and their solid solutions display a variety of exploitable properties. Frequently, distinct *B* cations mixed on the octahedral sites form ordered arrangements, and the properties of complex perovskites are strongly affected by the type, degree and spatial extent of this order. Examples of important perovskite-based materials whose functional responses depend critically on the *B*-cation order include relaxor ferroelectrics (Davies & Akbas, 2000; Burton *et al.*, 2006; Tinte *et al.*, 2006), microwave dielectrics (Davies, 1999), ion conductors (Norby, 2001) and piezoelectric systems with a morphotropic phase boundary (George *et al.*, 2003). Long-range *B*-cation order can be readily analyzed using superlattice reflections in X-ray or neutron diffraction patterns. However, in many cases of practical interest, the cation order is confined to the nanoscale, thereby yielding only diffuse intensity at the locations of superlattice reflections that cannot be detected by powder diffraction techniques. Single crystals suitable for the measurement of such diffuse X-ray or neutron scattering are unavailable for many perovskite systems of interest. While electron diffraction is effective in detecting ordered nanodomains, quantitative analyses of diffuse electron scattering are difficult. The situation becomes even more complicated for the cases of short-range order (SRO) where the diffuse intensity is distributed over reciprocal space rather than concentrated at the locations of the superlattice reflections, as might occur, for example, in $\text{Pb}(\text{Zr,Ti})\text{O}_3$ solid solutions. Extended X-ray absorption fine structure (EXAFS) can provide information regarding the *B*-cation SRO (Frenkel *et*

al., 2004; Laulhé *et al.*, 2006). However, the accuracy of EXAFS for tilted perovskites is strongly affected by photoelectron multiple scattering, which depends on the *B*–O–*B* angles and contributes to the EXAFS signal at distances similar to the *B*–*B* separation. Additionally, *B*-cation SRO parameters extracted from EXAFS are limited to the first *B*–*B* coordination shell. Therefore, alternative methods sensitive to local structure, amenable to quantification and applicable to polycrystalline materials are needed to determine the state of order in complex perovskites.

The pair-distribution function (PDF) from total scattering (Egami & Billinge, 2003) encodes local order characteristics. However, extracting chemical SRO information from the PDF presents a challenge even for relatively simple alloys, and few studies that deal with the metrological aspects of this problem have been reported. Proffen *et al.* (2002) used a Cu_3Au alloy to demonstrate that chemical SRO parameters can be extracted successfully from the total scattering PDF using a reverse Monte Carlo (RMC) algorithm (McGreevy & Pusztai, 1988). However, even the simplest $A(B',B'')\text{O}_3$ perovskite solid solutions are significantly more complicated than Cu_3Au . Firstly, *B*-cation ordering is accompanied by oxygen displacements which accommodate the cation size mismatch. Furthermore, this chemical ordering is often superimposed onto different types of displacive ordering, such as concerted cation (*A* and/or *B*) displacements and/or octahedral tilting.

Recently, we combined X-ray absorption spectroscopy (XAS) with neutron PDFs to probe the local structure and cation SRO in $\text{CaZr}_x\text{Ti}_{1-x}\text{O}_3$ (Levin *et al.*, 2006). This system exhibits two principal effects common for many perovskite solid solutions, namely a mixture of dissimilarly sized *B*

cations ($R_{\text{Ti}} \simeq 0.604 \text{ \AA}$ and $R_{\text{Zr}} \simeq 0.70 \text{ \AA}$) and octahedral tilting, which, along with a large difference in the neutron scattering lengths of Ti ($\bar{b} = -3.438 \text{ fm}$) and Zr ($\bar{b} = 7.16 \text{ fm}$), make it an attractive prototype for the study of local order. Simultaneous fits of the Ti and Zr *K*-edge EXAFS for $\text{CaZr}_{0.5}\text{Ti}_{0.5}\text{O}_3$ suggested a nearly random distribution of Ti and Zr. However, the uncertainty of ± 0.1 , reported for the probability of finding a Zr atom in the first *B*–*B* coordination sphere of Ti, was relatively large (Levin *et al.*, 2006). (This probability equals 0.5 and 1 for the random and fully ordered Zr/Ti arrangements, respectively.) Semi-quantitative analyses of PDFs and X-ray absorption near-edge structure (Krayzman *et al.*, 2006), while consistent with the EXAFS results, could not provide more accurate information.

In the present contribution, we have compared two RMC-based approaches for the extraction of the *B*-cation SRO parameters from the total scattering PDF. The first approach involves RMC refinements with a *B*-cation swap. The second approach, developed in the course of this study, combines RMC refinements with integration of the difference curve obtained by subtracting the fitted sum of all partial PDFs, except for those that describe the *B*–*B* correlations, from the experimental total PDF. We have applied both methods to the synthetic PDF calculated for differently ordered $\text{CaZr}_x\text{Ti}_{1-x}\text{O}_3$ and demonstrated that the second approach provides significantly more accurate values of the SRO parameters than the swap. Ultimately, we used this second method to analyze the *B*-cation SRO in real $\text{CaZr}_x\text{Ti}_{1-x}\text{O}_3$ samples.

2. Experimental

Ceramic samples of $\text{CaZr}_x\text{Ti}_{1-x}\text{O}_3$ ($x = 0, 1/4, 1/2, 3/4, 1$) solid solutions were prepared using a conventional solid-state synthesis, as detailed by Levin *et al.* (2006). The samples were equilibrated using multiple heat treatments (with intermediate grindings) at 1798 K for a total of 500 h until no changes in the X-ray diffraction line broadening could be observed. Neutron diffraction data for the PDF analyses were collected at ambient temperature on the NPDF instrument at the Lujan Neutron Scattering Center at LANSCE. The data corrections were carried out using the *PDFGETN* software (Peterson *et al.*, 2000). The total atomic PDF, $G(r)$, was obtained using a sine Fourier transform of the normalized scattering intensity, $S(Q)$. A Q_{max} of 40 \AA^{-1} was used. Ti and Zr *K*-edge EXAFS data for the $\text{CaZr}_x\text{Ti}_{1-x}\text{O}_3$ samples were collected at the Advanced Photon Source, as detailed by Levin *et al.* (2006).

RMC refinements were conducted using the *RMC-PROFILE* software (Tucker *et al.*, 2007). Structural models were generated using the *RMCPPOW* code (Mellergård & McGreevy, 1999) which incorporates local bond-valence sum (BVS) (Brown & Altermatt, 1985) constraints, thereby providing an efficient means for creating plausible models of perovskite solid solutions. All synthetic PDFs used in the present study were computed for neutron radiation. In this study, the *RMCPROFILE* code was modified to enable a simultaneous real-space fit of the PDF and single-scattering EXAFS data. The contributions of photoelectron single-

scattering paths to the EXAFS signal were calculated using the *FEFF6.0* code (Zabinsky *et al.*, 1995) as incorporated in the *ARTEMIS* software package (Ravel & Newville, 2005). The details of the algorithm for these combined PDF/EXAFS refinements will be reported elsewhere.

3. Results and discussion

3.1. *B*-cation SRO parameters in perovskites: definitions and relations to the total PDF

Similar to binary alloys, the *B*-cation chemical SRO in complex perovskites $AB'_xB''_{1-x}\text{O}_3$ can be conveniently described by the set of parameters $\alpha(k)$ (Cowley, 1950):

$$\alpha(k) = 1 - p(k)/x, \quad (1)$$

where $p(k)$ is the probability of finding a cation B' in the k th *B*–*B* coordination sphere of the cation B'' . Negative values of $\alpha(k)$ describe ordering (*i.e.* a preference for unlike neighbors), whereas positive $\alpha(k)$ correspond to clustering (a preference for similar neighbors). A random *B*-cation distribution yields $\alpha(k) = 0$. The range of possible values of $\alpha(k)$ for ordering varies with composition. For example, complete ordering in the first *B*–*B* coordination shell corresponds to $\alpha(1) = -1$ and $\alpha(1) = -0.33$ for $AB'_{0.5}B''_{0.5}\text{O}_3$ and $AB'_{0.75}B''_{0.25}\text{O}_3$, respectively. However, for clustering, the maximum value of $\alpha(k)$ remains equal to unity, regardless of composition.

A total atomic PDF, $G(r)$, can be defined as

$$G(r) = \sum_{i,j}^n c_i c_j \bar{b}_i \bar{b}_j [g_{ij}(r) - 1], \quad (2)$$

where c_i and c_j are the atomic fractions of species i and j in the material, \bar{b}_i and \bar{b}_j are the respective coherent neutron scattering lengths of these species, and $g_{ij}(r)$ is the partial i – j PDF. The summation in equation (2) is carried over all possible i – j pairs. The number of atoms j , $n_{ij}(r)$, located within the distance range ($r, r + dr$) from atom i can be calculated as

$$n_{ij}(r) = 4\pi\rho_0 c_j r^2 g_{ij}(r) dr, \quad (3)$$

where ρ_0 is the average number density of the material (atoms \AA^{-3}).

Let us denote the B' and B'' cations in $AB'_xB''_{1-x}\text{O}_3$ perovskites using the subscripts 1 and 2, respectively. All three partial PDFs, $g_{11}(r)$, $g_{12}(r)$ and $g_{22}(r)$, consist of well separated peaks, so that the coordination numbers $N_{11}(k)$, $N_{12}(k)$ and $N_{22}(k)$ (k refers to a sequential number of the *B*–*B* cation coordination shell) can be determined by integrating the corresponding $g_{ij}(r)$ peaks [equation (3)] as

$$N_{ij}(k) = \int_{r_{\text{min}}(k)}^{r_{\text{max}}(k)} n_{ij}(r) dr, \quad (4)$$

where $r_{\text{min}}(k)$ and $r_{\text{max}}(k)$ delimit the distance range for the k th *B*–*B* coordination shell. In perovskites, the following relations between the *B*–*B* coordination numbers hold:

$$N_{11}(k) + N_{12}(k) = N_{22}(k) + N_{21}(k) = N(k);$$

$$c_2 N_{21}(k) = c_1 N_{12}(k); \quad (5)$$

$$c_1 = 0.2x, c_2 = 0.2(1 - x);$$

where $N(k)$ is the total number of B cations in the k th coordination sphere of either the B' or B'' species. For example, $N(1) = 6$, $N(2) = 12$, etc.

The SRO parameters $\alpha(k)$ can then be expressed through the $N_{ij}(k)$ coordination numbers as

$$\alpha(k) = 1 - N_{21}(k)/xN(k) = 1 - N_{12}(k)/(1-x)N(k). \quad (6)$$

Unfortunately, partial B – B PDFs cannot be measured experimentally. However, one can recover the values of $N_{ij}(k)$ through the RMC fits of the total PDF. Below, we discuss the merits of the two distinct strategies for these fits.

3.2. RMC refinements with a B -cation swap

A straightforward approach for extracting $\alpha(k)$ from the total PDF involves an RMC refinement with a swap of the B' and B'' cations among the B sites. Previously, this approach proved successful for determining the chemical SRO in Cu_3Au (Proffen *et al.*, 2002). More recently, Hui *et al.* (2007) applied a swap algorithm to analyze the A -site SRO in $(\text{Ca},\text{Sr})\text{TiO}_3$ solid solutions and reported substantial local order of Ca and Sr for several compositions, although the accuracy of this procedure for perovskites has not been established. In the present contribution, we have assessed the accuracy of the swap method for the determination of the B -site SRO in perovskites by fitting synthetic PDFs for computer-generated models of $\text{CaZr}_{0.5}\text{Ti}_{0.5}\text{O}_3$ featuring different values of $\alpha(k)$ for the distribution of Zr and Ti (Fig. 1). Hereinafter, we refer to these synthetic PDFs, which play the role of experimental data, as the target PDFs.

All configurations consisted of 19360 atoms distributed in a box of dimensions $11a \times 8b \times 11c$, where $a = 5.6033$, $b =$

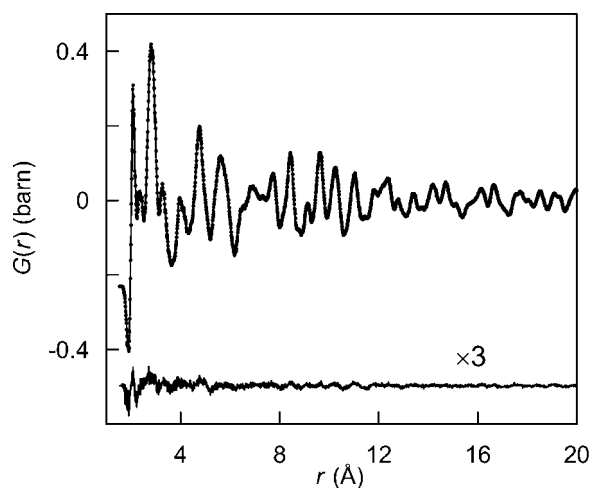


Figure 1

Top: target (circles) and fitted $G(r)$ (line) profiles for synthetic $\text{CaZr}_{0.5}\text{Ti}_{0.5}\text{O}_3$. Bottom: residual magnified by a factor of 3. The target configuration exhibits $\alpha(1) = 0$. The fit of $G(r)$ involved RMC refinements with a swap of Ti and Zr over the B sites. The refinements started from the average structure with $\alpha(1) = 0$. However, despite an excellent fit, the refined value of $\alpha(1)$ was -0.15 instead of 0. (1 barn = 10^{-24} cm².)

7.8295 and $c = 5.4870$ Å correspond to the experimental lattice parameters of $\text{CaZr}_{0.5}\text{Ti}_{0.5}\text{O}_3$. Configurations with distinct SRO were generated using a Monte Carlo swap of Zr and Ti among the B sites until the target values of $\alpha(1)$ and $\alpha(2)$ were attained. Subsequently, all atoms were allowed to move to satisfy the imposed local BVS criteria. The mean-square atomic displacements determined for the resulting configurations were consistent with the experimental displacement parameters obtained from crystallographic refinements. The procedure was used to generate several target structures with different sets of $\alpha(1)$ and $\alpha(2)$. The total PDFs calculated for these configurations were fitted using an RMC algorithm. During the fit, all atoms were allowed to move and either polyhedral or EXAFS constraints were imposed to ensure sensible B –O bond-length distributions. A series of fits was conducted, starting from the values of $\alpha(k)$ which deviated in positive (clustering) and negative (ordering) directions from the target.

Unconstrained RMC fits of the synthetic data yielded Ti–O and Zr–O distance distributions that were substantially broader and more distorted than their respective targets. Significantly better results were obtained using realistic polyhedral constraints (Tucker *et al.*, 2007) for the $[\text{BO}_6]$ octahedra. However, these constraints, as implemented in the current version of *RMCPROFILE*, are incompatible with a swap function. Concurrently, the combined RMC refinements using synthetic PDF and EXAFS (Ti and Zr K -edges), which are compatible with a swap, were very effective in correctly reproducing the target B –O partial PDFs without any *a priori* assumptions about the B –O distances (as introduced, for example, by the use of polyhedral constraints); the details of these combined refinements will be reported separately.

Despite an excellent fit of the total PDF (Fig. 1), the refined $\alpha(k)$ differed significantly from the target values. For example, even for initial and target configurations having identical $\alpha(1) = 0$, the refinements converged at $\alpha(1) = -0.15$. Thus, even in the absence of systematic errors, the RMC refinements with a B -cation swap yield significantly inaccurate results when using just the neutron PDF and EXAFS data. Part of the problem with a swap procedure when applied to perovskites is related to the good fit of the B –O peaks obtained even for somewhat incorrect values of $\alpha(k)$. As a result, further B – B swaps, which tend to degrade the B –O fit, become unfavorable and the swap freezes prematurely;¹ this effect is particularly strong for the neutron scattering data, in which the relative contribution of B –O pairs to the total PDF can substantially exceed that from the B – B pairs. Additionally, a prohibitively large number of RMC cycles are necessary to restore sensible oxygen positions around the swapped B cations. Note that a simultaneous fit of the neutron and X-ray PDFs with the EXAFS data improved the accuracy significantly: the refined values of $\alpha(1)$ ranged from -0.04 (starting from 0.49) to -0.07 (starting from -0.48) for the target $\alpha(1) = 0$. However, the

¹ Note that the situation is different in the case of $(\text{Ca},\text{Sr})\text{TiO}_3$ (Hui *et al.*, 2007), which features broad closely overlapped Ca–O and Sr–O peaks, instead of the relatively sharp well resolved Ti–O and Zr–O peaks in $\text{Ca}(\text{Zr},\text{Ti})\text{O}_3$.

data collection would require access to both pulsed neutron and high-energy X-ray sources. Below, we propose an alternative approach to swapping which significantly improves the accuracy of the $\alpha(k)$ values as determined just from the neutron total PDF.

3.3. RMC refinements with direct integration of the B - B contribution

For perovskites, the total PDF $G(r)$ can be written as

$$G(r) = \tilde{G}(r) + [c_1^2 \bar{b}_1^2 g_{11}(r) + 2c_1 c_2 \bar{b}_1 \bar{b}_2 g_{12}(r) + c_2^2 \bar{b}_2^2 g_{22}(r)], \quad (7)$$

where $\tilde{G}(r)$ is the sum of all partial PDFs apart from those that describe the B - B correlations, and $g_{11}(r)$, $g_{22}(r)$ and $g_{12}(r)$ are the B' - B'' partial PDFs, so that the sum in the square brackets represents the total B - B contribution to $G(r)$. For perovskite alloys $AB'_x B''_{1-x} O_3$ with a purely chemical B -site ordering (*i.e.* no accompanying atomic displacements), the SRO parameters $\alpha(k)$ can be determined by integrating the difference $G(r) - \tilde{G}(r)$ and using equations (5) and (6):

$$\alpha(k) = 1 + \frac{1}{(\bar{b}_1 - \bar{b}_2)^2} \left[\frac{5\Delta(k)}{x(1-x)N(k)} - \frac{\bar{b}_1^2}{(1-x)} - \frac{\bar{b}_2^2}{x} \right],$$

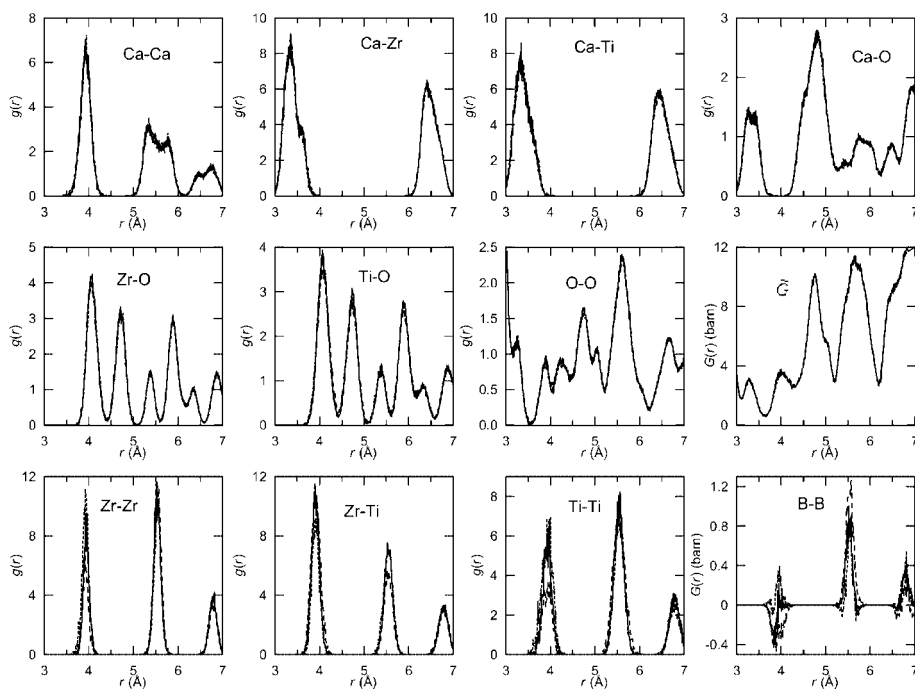


Figure 2

Partial $g_{ij}(r)$, $\tilde{G}(r)$ and the B - B contribution to the total $G(r)$ for the target (solid lines) and refined (dashed lines) configurations of $\text{CaZr}_{0.5}\text{Ti}_{0.5}\text{O}_3$. The target configuration exhibits $\alpha(1) = -0.25$ and $\alpha(2) = 0.1$. One of the refined configurations (short-dashed line) was built with a random Zr/Ti distribution [*i.e.* $\alpha(k) = 0$], whereas the other (long-dashed line) featured a significant degree of SRO [$\alpha(1) = -0.48$, $\alpha(2) = 0.28$]. Note that all partial $g_{ij}(r)$, apart from those that involve B - B pairs, were reproduced closely, regardless of the SRO parameters. Similarly, $\tilde{G}(r)$ exhibits relatively weak dependence on $\alpha(k)$.

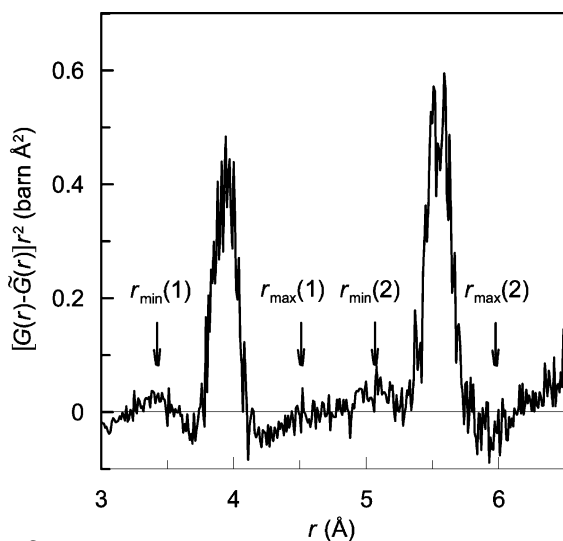
$$\begin{aligned} \Delta(k) &= 4\pi\rho_0 \int_{r_{\min}(k)}^{r_{\max}(k)} [G^{\text{exp}}(r) - \tilde{G}(r)] r^2 dr \\ &= c_1 \bar{b}_1^2 N_{11}(k) + 2c_1 \bar{b}_1 \bar{b}_2 N_{12}(k) + c_2 \bar{b}_2^2 N_{22}(k) \quad (8) \\ &= 0.2xN(k)\bar{b}_1^2 + 0.2(1-x)N(k)\bar{b}_2^2 \\ &\quad - 0.2xN_{12}(k)(\bar{b}_1 - \bar{b}_2)^2, \end{aligned}$$

where $G^{\text{exp}}(r)$ is the experimental total PDF and $\tilde{G}(r)$ can be calculated, for example, for a configuration with individual atoms displaced randomly from their average positions according to the displacement parameters obtained from crystallographic refinements.

In practice, B -site ordering involves additional displacements of all ions, and therefore the details of $\tilde{G}(r)$ will depend on the exact values of $\alpha(k)$. However, the integrals of all partial PDFs contributing to $\tilde{G}(r)$ still remain fixed by the perovskite stoichiometry. We performed RMC fits (without swap) of a synthetic PDF for $\text{CaZr}_{0.5}\text{Ti}_{0.5}\text{O}_3$ using two starting configurations with values of $\alpha(k)$ considerably different from the target. The results (Fig. 2) revealed that, for $r > 3$ Å, all partial PDFs (*i.e.* Ca-Ti, Ca-Zr, Ca-O, O-O) which overlap partly with the B - B peaks are closely reproduced even with significantly incorrect values of $\alpha(k)$. Those partial PDFs (*i.e.* Ca-Ca, Ti-O, Zr-O) that overlap nearly completely with the B - B peaks are more affected by $\alpha(k)$ (Fig. 2) because the fitting procedure modifies them to compensate for the

incorrect B - B contribution to $G(r)$. However, the peaks of these PDFs remain approximately confined within the integration limits of equation (8) and their integrals are known. Thus, within these integration limits, the integrals of $\tilde{G}(r)$ are reproduced closely enough [even for incorrect values of $\alpha(k)$] so that equation (8) can be used for the determination of $\alpha(k)$. As indicated above, the incorrect B - B contribution affects the shape and integrals of $\tilde{G}(r)$ because the fit minimizes the residual for the total $G(r)$; therefore, as the $\alpha(k)$ approach their correct values, the integrals of $\tilde{G}(r)$ over the B - B distance ranges improve as well.

We propose the following strategy for determining $\alpha(k)$. First, conventional crystallographic refinements of the structure are performed to determine lattice parameters, average atomic positions and atomic displacement parameters. The average structure is used to create an atomic configuration with the B' and B'' cations distributed over B sites according to some selected values of $\alpha(k)$. Then the PDF calculated for this configuration is fitted to the experimental data, and the results of


Figure 3

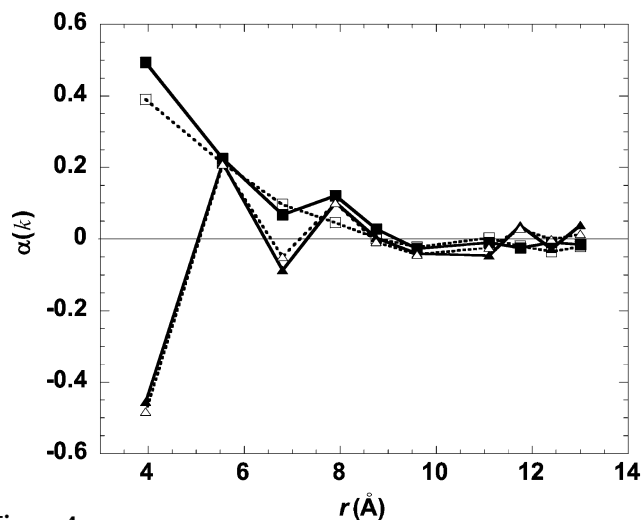
The product of r^2 and the difference between the total $G(r)$ for the target configuration of $\text{CaZr}_{0.5}\text{Ti}_{0.5}\text{O}_3$ and the $\tilde{G}(r)$ obtained by subtracting the B - B contribution from the RMC-fitted $G(r)$. Thus, the peaks at ~ 4 and ~ 5.6 Å reflect the B - B contributions for the first and second B - B coordination shells, respectively. The target configuration exhibits weak clustering with $\alpha(1) = 0.1$ and $\alpha(2) = 0.08$. The RMC was conducted for a configuration with $\alpha(k) = 0$ and all atoms located at the average positions. The integration limits $r_{\min}(k)$ and $r_{\max}(k)$ were selected to encompass the distance ranges for the B - B and Ca - Ca peaks in the corresponding partial PDFs. Selecting these limits at the zeroes of the derivative $d\{r^2[G(r) - \tilde{G}(r)]\}/dr$ minimizes errors caused by somewhat incorrect peak positions in the partial PDFs. Note that $r^2[G(r) - \tilde{G}(r)]$ is close to zero between the B - B peaks.

this refinement are used to calculate firstly $\tilde{G}(r)$ according to equation (7), then the difference $G^{\text{exp}}(r) - \tilde{G}(r)$ and, ultimately, the refined $\alpha(k)$ from equation (8). When the refined $\alpha(k)$ deviate significantly from the initial values, the next model is created with the new set of $\alpha(k)$, the RMC fit is repeated, and the resulting $\alpha(k)$ are extracted and compared with the corresponding values from the previous cycle. The procedure is iterated until the changes in $\alpha(k)$ remain within the preset error. In the following, we first test the proposed algorithm using the synthetic PDF for $\text{CaTi}_{0.5}\text{Zr}_{0.5}\text{O}_3$ and then apply it to the real experimental data for $\text{CaZr}_x\text{Ti}_{1-x}\text{O}_3$ solid solutions.

3.4. Determination of $\alpha(k)$ from the synthetic PDF

We tested the proposed approach by fitting the synthetic PDFs for the simulated target structures of $\text{CaZr}_{0.5}\text{Ti}_{0.5}\text{O}_3$ with distinct values of $\alpha(k)$ that mimicked either ordering or clustering. In the first example, we considered two target structures with weak SRO having $\alpha(1)/\alpha(2)$ values of $-0.1/0.08$ (ordering) and $0.1/0.08$ (clustering).² In both cases, the RMC fits were started from random configurations. The integration of $G^{\text{exp}}(r) - \tilde{G}(r)$ (Fig. 3) reproduced the SRO parameters, yielding $-0.1/0.07$ and $0.09/0.07$ for the cases of ordering and clustering, respectively; that is, a single iteration of the procedure was sufficient to recover nearly correct values of $\alpha(1)$ and $\alpha(2)$. Small systematic differences between the target

² For $k > 2$, $\alpha(k) \approx 0$.


Figure 4

Chemical SRO parameters, $\alpha(k)$, for successive B - B coordination shells in the synthetic models of $\text{CaZr}_{0.5}\text{Ti}_{0.5}\text{O}_3$ with strong local ordering (triangles) and clustering (squares). Solid symbols and the solid line denote $\alpha(k)$ for the target configuration. Open symbols and the dashed line denote $\alpha(k)$ retrieved from the neutron PDF using the iterative procedure proposed in the present study. Note that $\alpha(k)$ up to $k = 5$ (~ 8 Å) were recovered after two iterations of this procedure.

and recovered values of $\alpha(k)$ are caused by the approximations of the proposed method and some uncertainty in the selection of the integration limits in equation (8); typically, these differences are significantly larger than the statistical errors associated with the RMC procedure.

In the second example, we again selected two targets (clustering and ordering) but with much stronger SRO and correlation radii of ~ 8 Å (Fig. 4). Random starting configurations were used in the refinements. For such large differences between the $\alpha(k)$ values in the starting and target configurations, two iterations of the procedure were necessary. Fairly accurate values of $\alpha(k)$ were recovered up to $k = 5$ ($r \approx 8$ Å) for both ordering and clustering (Fig. 4).

Finally, in the third example, we considered a target with a moderate degree of SRO [$\alpha(1) = -0.25$, $\alpha(2) = 0.1$], while starting the fits from the configurations with $\alpha(1) = \alpha(2) = 0$ (*i.e.* random) and $\alpha(1) = -0.48$, $\alpha(2) = 0.28$ (*i.e.* strong ordering). A single iteration of our procedure yielded $(-0.21, 0.09)$ and $(-0.29, 0.12)$ for the random and ordered starting configurations, respectively; that is, the results converged to the correct values of $\alpha(k)$. Fig. 2 shows all fitted partial PDFs, along with the $\tilde{G}(r)$ and B - B contributions.

RMC refinements of $\text{CaZr}_{0.5}\text{Ti}_{0.5}\text{O}_3$ using neutron PDFs fail to reproduce accurately the details of the B - B peaks (*i.e.* positions/widths), even for configurations with the correct values of $\alpha(1)$ and $\alpha(2)$. In effect, the total residual, as defined by the difference between the experimental and fitted PDFs, provides little indication of the validity of the SRO parameters for the first few B - B coordination shells in the resulting configuration. Our procedure, which relies on the difference between the experimental and fitted integrals of $G(r)$ over the B - B distance ranges for the selection of the correct SRO parameters, is more sensitive to $\alpha(k)$ and relatively indifferent to other characteristics of the fitted model.

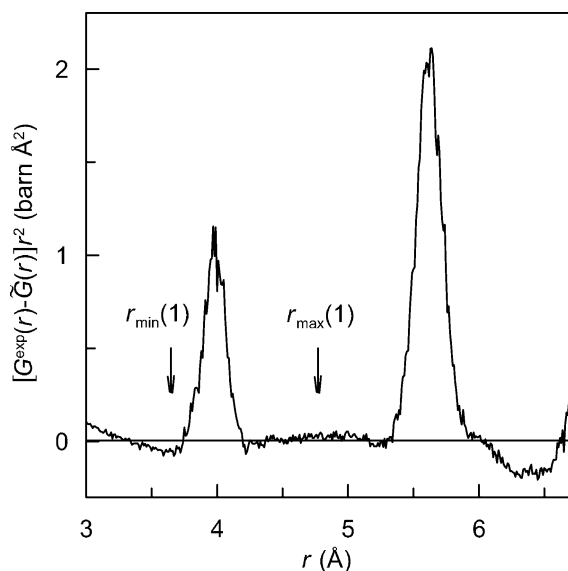


Figure 5

The product of r^2 and the difference between the total experimental $G(r)$ for $\text{CaZr}_{0.75}\text{Ti}_{0.25}\text{O}_3$ and the $\tilde{G}(r)$ obtained by subtracting the B - B contribution from the RMC-fitted $G(r)$. The RMC fit was conducted for a configuration with $\alpha(k) = 0$. The integration limits $r_{\min}(1)$ and $r_{\max}(1)$ used in the analyses are indicated by arrows.

Overall, these synthetic data analyses indicate that, in the absence of systematic errors, the proposed procedure enables accurate and robust determination of the B -cation SRO parameters from the neutron PDF, so that even the cases of weak ordering and clustering can be readily differentiated with high confidence. No statistically significant differences in the final values of $\alpha(k)$ were observed while using polyhedral constraints or a combined PDF/EXAFS fit.

3.5. Determination of $\alpha(k)$ from the experimental PDF for $\text{CaZr}_x\text{Ti}_{1-x}\text{O}_3$

Unlike the synthetic data, the experimental PDF contains systematic errors associated, at least in part, with the deficiencies of various corrections that have to be applied to the raw scattering data to extract a PDF. These systematic errors affect the accuracies of $\alpha(k)$ through the uncertainties in the values of the integrals $\Delta(k)$ [see equation (8)]. According to equation (8), these integrals decrease with increasing fraction of Ti because of a balance between the neutron scattering lengths of Zr and Ti; therefore, the relative uncertainties in the values of $\alpha(k)$ increase with x . We used the RMC fits to the PDF data of the end compounds CaTiO_3 and CaZrO_3 with known coordination numbers to assess the magnitudes of these errors. The analyses were limited to the first B - B coordination shell. The errors were substantially larger for CaTiO_3 , presumably due to the weak coherent neutron scattering cross section of Ti which, combined with its relatively large absorption cross section, exacerbates the inaccuracies of multiple scattering and absorption corrections. The systematic correction to the calculated value of $\alpha(1)$ for the solid solutions $\text{CaZr}_x\text{Ti}_{1-x}\text{O}_3$ with $x \leq 1/2$, as estimated from the errors in $\Delta(1)$ for CaZrO_3 and CaTiO_3 , does not exceed 0.1.

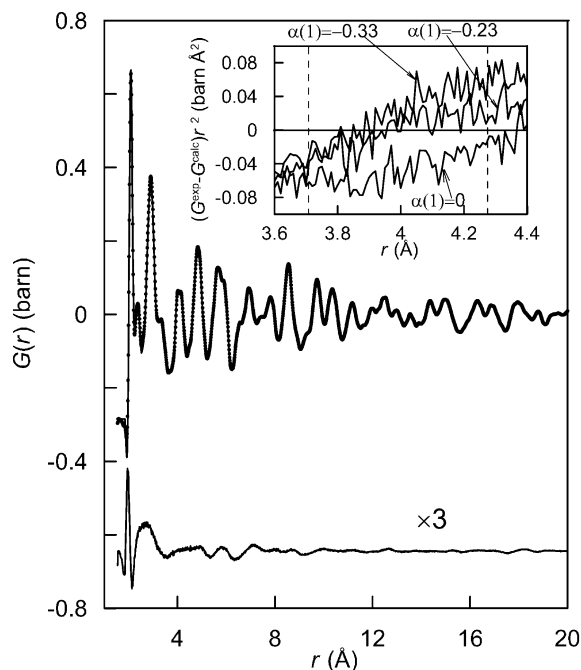


Figure 6

Top: experimental (circles) and calculated (line) $G(r)$ for $\text{CaZr}_{0.25}\text{Ti}_{0.75}\text{O}_3$. The calculated $G(r)$ corresponds to a configuration with $\alpha(1) = -0.23$. Bottom: residual multiplied by a factor of 3. Inset: residual (multiplied by r^2) over the distance range of the first B - B peak, as indicated by vertical dashed lines, for different values of $\alpha(1)$. Note that the residual integral over this distance range is minimal for $\alpha(1) = -0.23$.

However, for $x > 1/2$, significantly larger errors are expected. Therefore, we limited the analyses to the compositions $\text{CaZr}_{0.25}\text{Ti}_{0.75}\text{O}_3$ and $\text{CaZr}_{0.50}\text{Ti}_{0.50}\text{O}_3$.

For $\text{CaZr}_{0.75}\text{Ti}_{0.25}\text{O}_3$, the fit that was started from the initial atomic configuration having a random distribution of Zr and Ti atoms yielded $\alpha(1) = -0.16$ (2),³ which suggested a tendency towards ordering (Fig. 5). The second iteration starting from the model with $\alpha(1) = -0.16$ produced $\alpha(1) = -0.22$ (2), while the third iteration from $\alpha(1) = -0.23$ converged to $\alpha(1) = -0.22$, which was, therefore, taken as the SRO parameter. A fit that was started from the maximum possible $\alpha(1) = -0.33$ returned $\alpha(1) = -0.24$ (2). The value of $\alpha(1) = -0.22$ is significantly larger than the estimated systematic error. The results of the PDF fit for the configuration with $\alpha(1) = -0.23$ are shown in Fig. 6. No significant difference in the agreement factors over the fitted distance range was observed, regardless of the values of $\alpha(1)$; that is, the fitting statistics cannot be used as an indicator of the correct SRO parameters.

Similar iterative analyses for $\text{CaZr}_{0.5}\text{Ti}_{0.5}\text{O}_3$ (Fig. 7), with starting values of $\alpha(1)$ ranging from 0 to -0.82 , converged to $\alpha(1) = -0.28$ (2), again suggesting a weak ordering of Zr and Ti. This value of $\alpha(1)$ corresponds to a probability of finding Zr in the first B - B coordination shell of Ti of 0.64, as opposed to the random value of 0.5. This deviation from randomness is

³ The number in parentheses reflects the maximum uncertainty in $\alpha(1)$ introduced by uncertainties in the choice of r_{\min} and r_{\max} in equation (8).

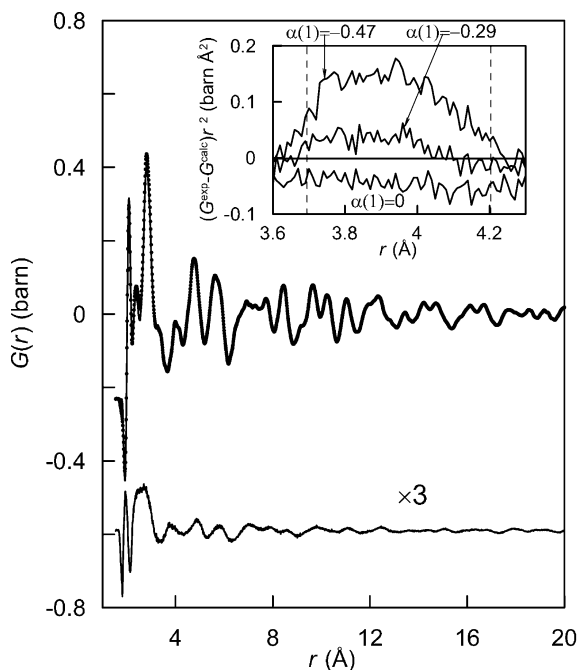


Figure 7
 Top: experimental (circles) and calculated (line) $G(r)$ for $\text{CaZr}_{0.5}\text{Ti}_{0.5}\text{O}_3$. The calculated $G(r)$ corresponds to a configuration with $\alpha(1) = -0.29$. Bottom: residual multiplied by a factor of 3. Inset: residual (multiplied by r^2) over the distance range of the first B - B peak, as indicated by vertical dashed lines, for different values of $\alpha(1)$. Note that the residual integral over this distance range is minimal for $\alpha(1) = -0.29$.

too small to be detected reliably using EXAFS. Note that the actual value of $\alpha(1)$ can be somewhat reduced because of the systematic errors which are substantial at this composition. However, the weak trend towards ordering of Zr and Ti appears to be significant. As in the case of the synthetic data, statistically similar results were obtained when using the combined PDF/EXAFS fits and the PDF fits with polyhedral constraints.

4. Conclusions

We have compared two distinct RMC-based approaches for the extraction of the B -cation SRO parameters in perovskite solid solutions from the total scattering PDF. The first, more traditional, approach involves a B -cation swap, whereas the second method, developed in the present study, relies on the iterative integration of the difference curve obtained by subtracting the fitted sum of all partial PDFs, except for those that describe the B - B correlations, from the experimental total PDF. This latter approach relies on the assumption that the sum of all partial PDFs apart from the B - B is recovered closely within the distance ranges for the B - B peaks, even with

incorrect values of the B -cation SRO parameters in the starting model. We have applied both methods to the synthetic PDF generated for differently ordered $\text{CaZr}_x\text{Ti}_{1-x}\text{O}_3$ and demonstrated that the second approach provides significantly more accurate values of the SRO parameters than the traditional swap. We have used this second method to analyze the B -cation SRO in real $\text{CaZr}_x\text{Ti}_{1-x}\text{O}_3$ ($x = 1/2, 3/4$) samples. The results revealed the presence of a weak but discernible local order of Zr and Ti that could not be detected reliably in the previous EXAFS analyses.

The authors are grateful to Thomas Proffen (LANL) for technical assistance with collecting the neutron diffraction data, and to Matthew Tucker (ISIS) for providing the source code of *RMCPROFILE*. Some of the samples were prepared by Michael Lufaso (UNF).

References

- Brown, I. D. & Altermatt, D. (1985). *Acta Cryst.* **B41**, 244–247.
 Burton, B. P., Cockayne, E., Tinte, S. & Waghmare, U. V. (2006). *Phase Transit.* **79**, 91–121.
 Cowley, J. M. (1950). *J. Appl. Phys.* **21**, 24–30.
 Davies, P. K. (1999). *Curr. Opin. Solid State Mater. Sci.* **4**, 467–471.
 Davies, P. K. & Akbas, M. A. (2000). *J. Phys. Chem. Solids*, **61**, 159–166.
 Egami, T. & Billinge, S. J. L. (2003). *Underneath the Bragg Peaks, Structural Analyses of Complex Materials*. New York: Pergamon.
 Frenkel, A. I., Pease, D. M., Giniewicz, J., Stern, E. A., Brewe, D. L., Daniel, M. & Budnick, J. (2004). *Phys. Rev. B*, **70**, 014106.
 George, A. M., Íñiguez, J. & Bellaiche, L. (2003). *Phys. Rev. Lett.* **91**, 045504.
 Hui, Q., Dove, M. T., Tucker, M. G., Redfern, S. A. T. & Keen, D. A. (2007). *J. Phys. Condens. Matter*, **19**, 335214.
 Krayzman, V., Levin, I., Woicik, J. C., Yoder, D. & Fischer, D. A. (2006). *Phys. Rev. B*, **74**, 224104.
 Laulhé, C., Hippert, F., Kreisel, J., Maglione, M., Simon, A., Hazermann, J. L. & Nassif, V. (2006). *Phys. Rev. B*, **74**, 014106.
 Levin, I., Cockayne, E., Lufazo, M. W., Woicik, J. C. & Maslar, J. E. (2006). *Chem. Mater.* **18**, 854–860.
 McGreevy, R. L. & Pusztai, L. (1988). *Mol. Simul.* **1**, 395–467.
 Møllergård, A. & McGreevy, R. L. (1999). *Acta Cryst.* **A55**, 783–789.
 Norby, T. (2001). *J. Mater. Chem.* **11**, 11–18.
 Peterson, P. F., Gutmann, M., Proffen, Th. & Billinge, S. J. L. (2000). *J. Appl. Cryst.* **33**, 1192.
 Proffen, Th., Petkov, V., Billinge, S. J. L. & Vogt, T. (2002). *Z. Kristallogr.* **217**, 47–50.
 Ravel, B. & Newville, M. (2005). *J. Synchrotron Rad.* **12**, 537–541.
 Tinte, S., Burton, B. P., Cockayne, E. & Waghmare, U. V. (2006). *Phys. Rev. Lett.* **97**, 137601.
 Tucker, M. G., Keen, D. A., Dove, M. T., Goodwin, A. L. & Hui, Q. (2007). *J. Phys. Condens. Matter*, **19**, 335218.
 Zabinsky, S. I., Rehr, J. J., Ankudinov, A., Albers, R. C. & Eller, M. J. (1995). *Phys. Rev. B*, **70**, 2995–3009.